

# Atomic decoration for improving the efficiency of field electron emission of carbon nanotubes

Guohua Chen, Zhibing Li,\* Jie Peng, Chunshan He, Weiliang Wang,  
Shaozhi Deng, and Ningsheng Xu†

*State Key Laboratory of Optoelectronic Materials and Technologies School of  
Physics and Engineering, Sun Yat-Sen University, Guangzhou 510275, China*

Chongyu Wang and Shanying Wang  
*Department of Physics, Tsinghua University, Beijing 100084, China*

Xiao Zheng and GuanHua Chen  
*Department of Chemistry, the University of Hong Kong, Hong Kong, China*

Tao Yu  
*Central Iron and Steel Research Institute, Beijing, China*  
(Dated: May 25, 2019)

The field electron emission from single-walled carbon nanotubes with their open ends decorated by -O, -BH and -NH, respectively, has been simulated. The apex-vacuum barrier and the emission current have been calculated. It was found that -BH and -NH suppress the apex-vacuum barrier significantly and lead to higher emission current in contrast to the -O terminated structure in the same applied field. The calculated binding energies show that the tubes with -BH and -NH endings are much stable than both the oxygen and hydrogen saturated tubes.

PACS numbers:

## I. INTRODUCTION

The field electron emission (FE) from carbon nanotubes (CNTs) have found its applications in flat panel displays [1], in molecular sensors [2, 3, 4], and in miniature high-brightness electron sources for both electron microscope [5] and parallel e-beam lithography system [6]. One of the central problems in these applications is to improve the efficiency of FE. It was once believed that the large aspect ratio of a CNT that would lead to large local field enhancement (LFE) at the apex of the CNT were the major reason for the superior FE, thereby it would be straight forward to improve FE efficiency by increasing the length of the CNT. But this common view has not been verified. Recent simulations have shown that the charge accumulation in both the apex and the body of CNTs has important effects on the apex-vacuum barrier (AVB) and thereby on the FE characteristics [7, 8]. The field enhancement factor for open SWCNT is much smaller than expected value of the classical metal wire model; on the other hand, the change of the AVB has more pronounced effect to FE [9].

The change of AVB should be originated from the size effects of the nanoscopic CNT emitter, where the atomic structure of the apex has strong influence to the FE process. It has been observed that the hydrogenation of the tube wall transforms a metallic CNT to a semiconducting one [10], that O<sub>2</sub> exposure increases the turn-on field of SWCNTs and decreases the FE efficiency [11], and that the adsorption of H<sub>2</sub>O enhances the field emission current [12]. However, experimental observations so far have not been conclusive

[13, 14, 15]. To understand the dependence of FE upon the atomic structures of apexes of CNTs, careful simulations via the density functional method (DFT) have been carried out [16, 17, 18, 19, 20, 21, 22]. There are contradictory conclusions about the effect of adsorbates. Zhou et al [23] and Kim et al [24, 25] obtained the local density of states (LDOS) at the apex by ab initio methods; they found that the LDOS at the charge-neutrality level was suppressed by the hydrogen. They therefore concluded that hydrogen adsorption reduces FE current density. By contrast, Mayer et al. calculated the AVB using a dipole and point charge model [25]; they assumed that the apex-vacuum barrier was reduced by the presence of the hydrogen, and concluded that hydrogen adsorption enhances the FE current density. Mayer recently improved the model and illustrated the electrostatic potential around the carbon nanotube [10]. More careful studies on this topic would obviously be useful.

Only recently, it is possible to tackle the realistic size of SWCNTs in FE conditions by a multi-scale method involving quantum mechanics and molecular mechanics [26, 27]. In the present paper, we adopted this method to simulate the FE from SWCNTs of realistic length (one micrometer) with atomic decorations at the open end. The purpose of this study is to optimize the apex structure of the SWCNT to achieve higher FE efficiency. Obviously the AVB and thereby the FE characteristic will be strongly affected by the electron transfer among carbons and adsorbate atoms. The atomic decoration and geometric symmetry breaking in the apex will lead to formation of dipoles and quadrupoles (referred to as spontaneous multipoles). If the dipole has its positive end outward to the vacuum (positive dipole), it tends to suppress the AVB; otherwise (negative dipole), it tends to raise the barrier. This simple argument suggests that the carbon dangling bonds in the opened end of the SWCNT should be saturated by atoms of

\*Electronic address: stslzb@zsu.edu.cn

†Electronic address: stsns@zsu.edu.cn

TABLE I: Electronegativity of related atoms.

atom	H	B	C	N	O
$X_S$	2.300	2.051	2.544	3.066	3.610

lower electronegativity (denoted by  $X_S$ ) in contrast with carbons. For instance, the hydrogen terminated SWCNT has a positive dipole because the hydrogen has lower  $X_S$  than the carbon [9].

Besides hydrogen, boron could be a candidate of decoration atom for creating positive dipoles in the apex since boron has lower  $X_S$  relative to carbon. In room temperature, the electrons to be emitted to vacuum would likely come from states localized in the vicinity of the free end. Therefore, higher density of electrons in the apex would mean more incident electrons hitting the AVB. To attract electrons from the tube column to the apex, it would be useful to insert an atom with higher  $X_S$  in between the last carbon and the low  $X_S$  atoms. For instance, the nitrogen can be such a medium atom since its  $X_S$  is higher than carbon. Another consideration is the structural stability that is usually appealed in applications. The present simulations have shown that the -BH and -NH adsorbates have larger binding energy than both oxygen and hydrogen. For these reasons, we are interested in SWCNTs terminated by atom-pairs -BH and -NH. For comparison, we also studied the tube terminated by oxygen atoms that has high  $X_S$ . The negativities of hydrogen, boron, carbon, nitrogen, and oxygen are given in Table 1.

We adopted the multi-scale method [26, 27] to simulate the (5, 5) SWCNT with -BH, -NH and -O as ending atoms (atom pairs) respectively. The AVB that is most important for the FE was obtained. Reduced AVB as the essential mechanism, besides the effect of the LFE, was confirmed to be responsible for the low turn-on field of CNTs. In Section II, the simulation method will be reviewed briefly. The charge density and electrostatic potential in the absence of applied field will be given in Section III. In Section IV, the field-depending AVBs will be illustrated. The easiest path for field electron emission has been studied and the emission characteristics of the (5, 5) SWCNT with -BH, -NH and -O endings have been given in Section V. The last section will be devoted to the discussions and conclusions.

## II. SIMULATION METHOD AND THE ENDING STRUCTURES

The concept of multi-scale coupling is important to simulations of huge systems that are sensitive to all scales of the systems [28, 29]. The CNTs for the purpose of FE are typical multi-scale systems. A simplified schematic setup of FE system is shown in Fig.1, in which two black plates are the cathode (left) and anode (right) respectively; a CNT is grown vertically on the cathode. Applying a voltage to the gate, electrons will have opportunity to emit into vacuum through the apex of the CNT by quantum tunneling.

In experiments, the length of CNTs is usually in microme-

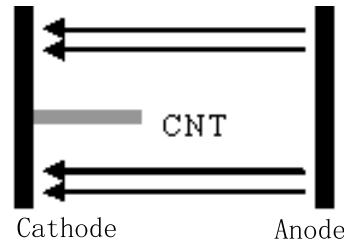


FIG. 1: The schematic setup of field electron emission. The arrow lines represent the applied electric field.

ters, while the radius is in nanometers. For instance, the (5, 5) type SWCNT of one micrometer long consists about carbon atoms. It is still impossible to deal the entire system with the first principle methods. Limited by the computational efficiencies and resources, all ab initio studies so far can only simulate the local properties involving hundreds of carbon atoms. As the electronic properties are sensitive to both the detail atomic arrangement (i.e. the location of defects and adsorbates) and the electron states, which would extend over the whole tube, it is a big challenge to computer simulations.

Since electrons are emitted from the apex of the SWCNT by quantum tunneling, the part including the apex of the SWCNT must be treated by quantum mechanics. The part on the substrate side mainly affects the FE through Coulomb potential of the excess charge, so that it can be treated by a semi-classical method [26, 27]. Therefore we divided the SWCNT into a quantum region and a semi-classical region. The quantum region was simulated in atomic scale where the density matrix of electron was obtained quantum mechanically. In the semi-classical region, the Coulomb potential is governed by the Poisson equation.

It should be noted that even in the semi-classical region the electron energy band structure originated from quantum mechanics should be taken into account. The excess charge distribution in the semi-classical region has simple solution only for simple band structure. For the (5, 5) SWCNT, there are both experimental and theoretical evidences for the constant density of state (DOS) in the vicinity of neutrality level [30, 31]. Hence the semi-classical region should be limited in the region where the constant DOS is valid. To our experience, this means that the length of the quantum region should be over 100nm.

In the present simulation, the quantum region extends 123nm and contains 10,000 atoms. It is still too big for an ab initio simulation. The quantum region is then farther divided into sub-regions. Each sub-region and its adjacent sub-region form a subsystem that is simulated by the modified neglect of diatomic overlap (MNDO) semi-empirical quantum mechanical method (here the Mopac software was used). The excess charges in the quantum region but not in the subsystem being simulating are treated as point charges. Their contribution to the subsystem being simulating is through Coulomb interaction.

The coupling of quantum region and semi-classical region is through the quasi-thermodynamic equilibrium condition which assumes that the electrochemical potential (Fermi

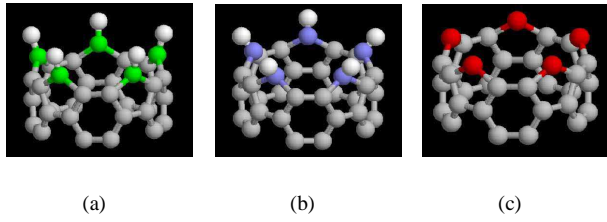


FIG. 2: Three ending structures of a (5, 5) SWCNT. The gray balls stand for carbon atoms. (a) The a-type structure with -BH adsorbates. The green balls stand for boron atoms and white balls for hydrogen atoms. (b) The b-type structure with -NH adsorbates. The blue and white balls denote nitrogen atoms and hydrogen atoms, respectively. (c) The c-type structure with oxygen adsorbates. The red balls stand for oxygen atoms.

level) is a constant along the nanotube, and equal to that of the substrate. The densities of the excess charge ("excess density" for simplicity) calculated separately in quantum and semi-classical regions should coincide at some overlap place of two regions. Here we required that the excess densities coincide at  $z = 900\text{nm}$ . The self-consistent excess density of the entire CNT is achieved by a small loop and a big loop. In the smaller loop, the sub-regions of the quantum region are simulated one by one, and repeated until a converged electron density of the quantum region is obtained. The big loop is an alterative simulation of quantum region and the semi-classical region. This process is greatly accelerated by the observation of that the charge density in the region far from the apex is, to a good approximation, a linear function of the distance from the substrate. This linear behavior is a consequence of the constant DOS in the classical region [32].

When the SWCNT is mounted on the metallic substrate, Schottky junction will be formed at the back contact. However, as the apex properties are mostly concerned for FE, this junction could be ignored. Equivalently, we have assumed that the Fermi level of the isolated SWCNT aligns with the Fermi level of the metal. The boundary condition of the metal surface is guaranteed by the image charges of the excess charges of the SWCNT. The total electrostatic potential is the superposition of the Coulomb potential created by excess charges and their images in the substrate, as well as the applied macroscopic field.

The apex structures with -BH, -NH, and -O terminations are shown in Fig. 2, they will be referred to as a-type, b-type, and c-type structures respectively. The five green balls in Fig. 2 (a) for the a-type structure stand the boron atoms. Each boron atom shares two bonds with two carbon atoms respectively. The third bond of boron atom is saturated by a hydrogen atom (the white ball). Similarly, the b-type structure is shown in Fig. 2 (b), with the blue balls for nitrogen atoms and white balls for hydrogen atoms. The five oxygen atoms are represented by red balls in Fig. 2(c) for the c-type structure. All ending structures have been relaxed by the MOPAC software. The coordinates of ending atoms and the first layer of carbons are given in Table 2.

TABLE II: The coordinates of the adsorbates and carbons of the top layer.

Structures	Coordinate (angstrom)		
	X	Y	Z
-BH	H	10088.04	2.35
	B	10086.92	2.10
	C	10086.04	0.94
-NH	H	10087.60	2.35
	N	10086.87	1.91
	C	10086.04	0.94
-O	O	10086.83	2.05
	C	10086.04	0.94

TABLE III: The binding energy of each adsorbate atom (or cluster).

Adsorbate atom (cluster)	-BH	-NH	-O	-H
Binding energy(eV)	17.8	18.3	3.99	8.63

The binding energy is defined as the energy with the adsorbates separated from each other and from the carbons in large distance subtracted by the energy with adsorbates forming bonds with carbons. In the calculations of binding energies, we only considered the last ten layers of carbons at the tips. The stability of the ending structure is described by the binding energy per adsorbate atom (or cluster). The results are shown in Table 3. The a-type and b-type ending structures are obviously more stable than the c-type and the structure in which every carbon dangling bond is saturated by a hydrogen atom.

### III. ELECTRONIC STRUCTURES IN THE ABSENCE OF APPLIED FIELD

The FE characteristic of each individual SWCNT should be relied on its intrinsic electronic structure. Therefore in this section we will focus at the electronic structure of the SWCNTs in the absence of external macroscopic field.

Figure. 3 (a)/(b)/(c) show the electron densities in the intersection plane, on which the axis of SWCNTs and one boron/nitrogen/oxygen atom are located. The X in Fig. 3 is the radial coordinate, i.e. the distance (in angstrom) from the axis. The coordinate Z denotes the distance (in angstrom) from the substrate. The arrows mark positions of the adsorbate atoms. For the a-type structure (Fig. 3 (a)), obviously the electrons transfer from boron atoms to hydrogen atoms. By Fig. 3 (b) one can see that the electrons in the b-type ending are concentrated at the nitrogen atoms. While for the c-type structure (Fig. 3 (c)), electrons are strongly concentrated at oxygen atoms. This fact can be seen more clearly in Fig. 4, where the distribution of excess electrons along the wall of SWCNT is shown. The excess charges associated to each atom of the top three(two) layers of a-type/b-type(c-type) structures have been calculated by the Mulliken population analysis method. The results are given in the second column of Table 4.

TABLE IV: The distribution of the excess charges.

cluster	Excess charges (e)
CBH	-0.082(C), 0.276(B), -0.039(H)
CNH	0.086(C), -0.248(N), 0.150(H)
CO	0.182(C), -0.302(O)

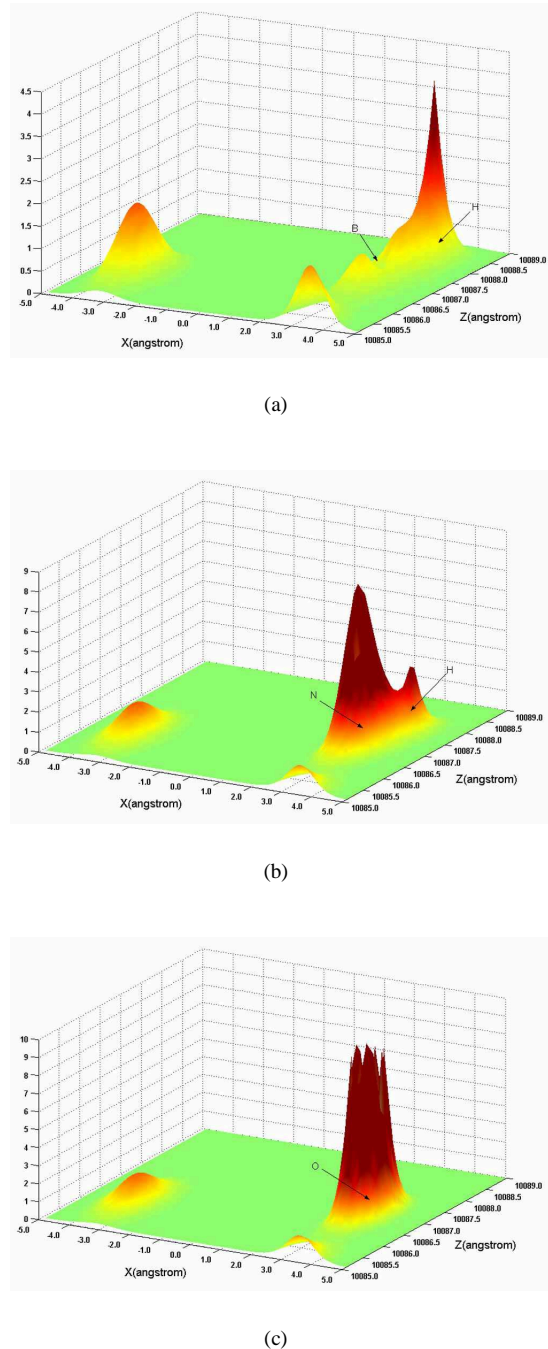


FIG. 3: The distribution of electrons on the intersection plane crossing one adsorbate atom and the axis of the SWCNT. (a), (b), and (c) are for a-, b-, and c-type ending structures respectively.

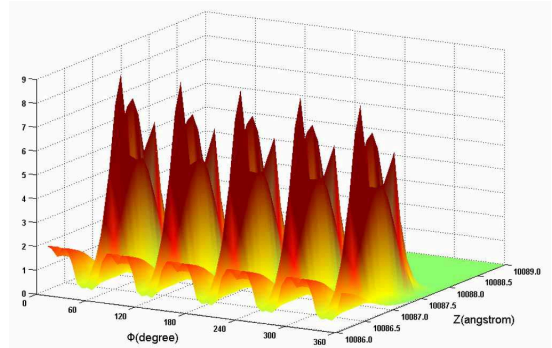


FIG. 4: The electron distribution around the last two layers of atoms of the SWCNT terminated with oxygen.

#### IV. FIELD-DEPENDING BARRIER

Now let us investigate the consequences of applied macroscopic fields  $F_{appl}$ . The general picture is as follows. The applied field  $F_{appl}$  drives electrons to the tip of the SWCNT until the equilibrium is set up. We have assumed that the emission current is weak and can be ignored in the calculation of electron density in the SWCNT. The re-distribution of electrons in  $F_{appl}$  has two consequences. Firstly, the field is shielded in the body of the tube, more or less, that leads to the field enhancement at the tip. However, as the SWCNT has only one layer of atoms, the shielding is not complete especially in the tip region where the field is strong. There is field penetration in the tip region, so the field enhancement factor is smaller than predicted by the classical theory for a metal rod. Secondly, there are excess charges accumulating along the tube, especially in the tip. In the quasi-equilibrium assumption, the charge accumulation is only possible if the neutrality energy level of the SWCNT bends down. This happens because that the applied field lowers the energies of local orbitals. The orbital with energy between the Fermi level of the substrate and the neutrality energy level can accommodate electrons and contribute excess charges.

The superposition of Coulomb potential of all charges in the tube and their images in the substrate together with the potential of  $F_{appl}$  determines the AVB for the electron emission. In Fig. 5(a), we plot the electron energy potential  $U(z)$  of the a-type structure for various  $F_{appl}$ . The z axis has its origin at the last atom of the SWCNT and is parallel to the direction of tube axis. The dependence of AVB on  $F_{appl}$  is significant. The barrier potential  $U(z)$  of three ending structures are compared in Fig. 5(b) for  $F_{appl} = 7.0 \text{ V/m}$ . The b-type has smaller AVB, implying a higher emission current (see next section).

The field enhancement factor as a feature of the AVB is highly concerned in FE applications. For the SWCNTs, however, it is difficult to define a quantity that corresponds exactly to the field enhancement factor as usually defined for planar metallic emitters. Denote the maximum local field by  $F_{appl}$ . Here the field enhancement factor  $\gamma_q$  is defined as  $F_{apex}/F_{appl}$ . The variation of this field enhancement factor with the value of  $1/F_{appl}$  is shown in Fig. 6. Note that  $\gamma_q$  of these structures

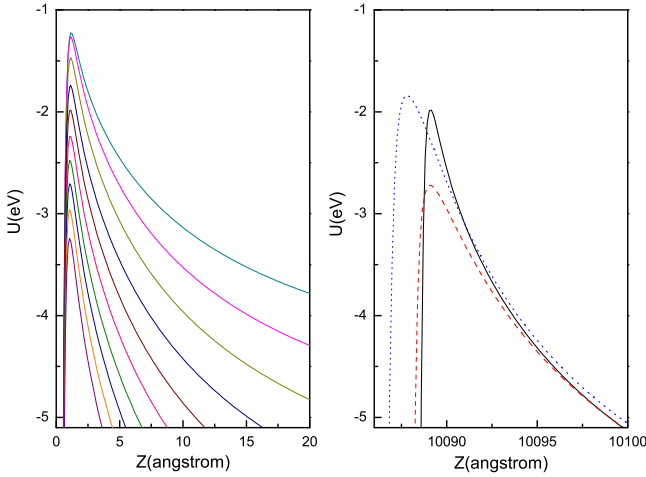


FIG. 5: The AVBs in front of SWCNTs. (a)  $U(z)$  of a-type structure in  $F_{appl}$  from  $6.0V/m$  to  $15.0V/m$ , with step  $1.0V/m$ . The lower barrier is corresponding to larger  $F_{appl}$ . (b)  $U(z)$  of three ending structures in the applied field of  $7.0V/m$ . The solid, dashed, and dotted curves are corresponding to the a-type, b-type, and c-type structures.

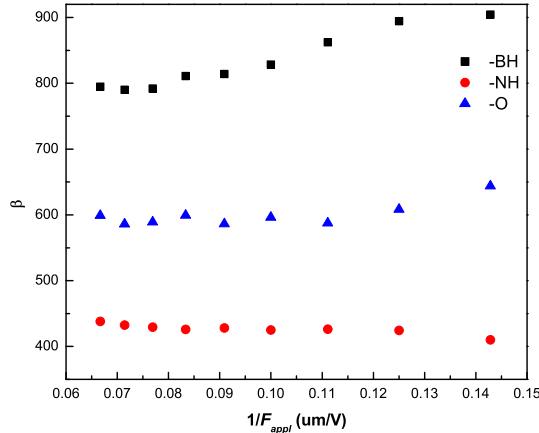


FIG. 6: The field enhancement factor varies as the inverse of applied field. The squares, the circles, and the triangles are data of the simulations for a-, b-, and c-type structures, respectively.

do not change significantly, but are obviously different from each other. It shows the important influence of adsorbate in FE.

## V. EMISSION CURRENTS AND EMISSION PATHS

Quantum mechanically, any emission path has a probability amplitude for electron emission. In the semi-classical approximation, only the path along which the barrier is the weakest should be relevant. This path will be referred to as the easiest path. Since both the a-type and b-type ending structures have the thinnest AVB in front of the hydrogen atoms, the easiest paths of these structures should start from the hydrogen atoms. The thinnest AVB of the c-type structure starts from top carbon atoms outward along a path in between two

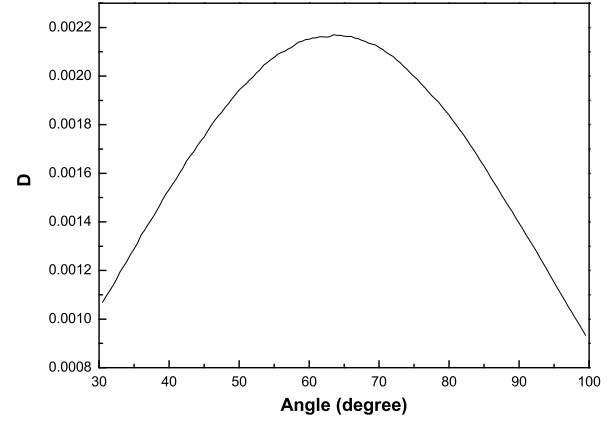


FIG. 7:  $D$  versus the path angles for a-type ending structure in  $12V/m$ .

oxygen atoms. For simplicity, we assumed that electrons go through the barrier in straight lines. Along the easiest path, the transmission coefficient can be estimated by the WKB approximation,

$$D(E_F) = \exp\left[-\frac{2}{\hbar} \text{Im} \int \sqrt{2m[E_F - V(z)]} dz\right] \quad (1)$$

The electron possessed the Fermi level was assumed. If the path was not the easiest path, the value of Eq. (1) should be smaller. For instance, Fig. 7 shows the  $D$  versus the path angle for a-type ending structure in  $12V/m$ . The angle of the easiest path was determined by the maximum of  $D$ . Since the AVB is field-dependent, the easiest path would change its orientation with the applied fields. The angles of the easiest paths versus applied fields were plotted in Fig. 8. The squares, circles, and triangles are for a-type, b-type, and c-type structures, respectively. The curves in Fig. 8 have the general trend that the angles of the easiest paths decrease as the applied field increases. This phenomenon would be related to the electron accumulation at the top layers of atoms.

With the transmission coefficient in hand, the emission current was estimated by,

$$I = \nu q_{exc} D(E_F) \quad (2)$$

Where  $q_{exc}$  are the extra electrons at atoms from which the easiest paths start,  $\nu$  the collision frequency that can be estimated from the average kinetic energy of  $\pi^*$  electrons, to  $\nu = E_k(\pi^*)/h$ . Another way to estimate the collision frequency is to use the uncertainty relation,

$$\nu = \frac{E_k}{h} = \frac{h}{32\pi^2 m \langle \Delta r^2 \rangle} \quad (3)$$

where  $\langle \Delta r^2 \rangle$  is the uncertainty of the radial coordinate. Its numerical value could be estimated from the density of excessive electrons (Fig. 3). The collision frequency estimated by two methods has the same order,  $10^{14} \text{Hz}$ .

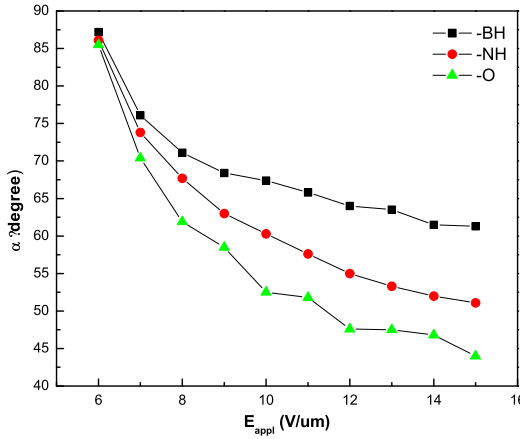


FIG. 8: The angles of the easiest paths versus applied fields. The squares, the circles, and the triangles are for a-, b-, and c-type structures, respectively.

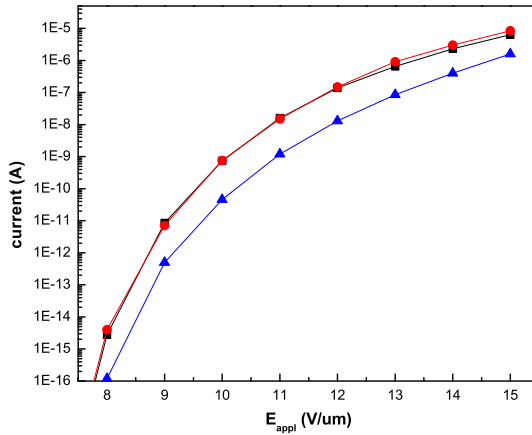


FIG. 9: The currents versus applied fields. The, squares, circles, and triangles are corresponding to currents of a-, b-, and c-type structures, respectively.

Fig. 9 shows the emission currents of a-type (squares), b-type (circles), and c-type (triangles) structures.

## VI. CONCLUSIONS

The one micrometer long (5, 5) single wall carbon nanotube is simulated by the multi-scale method. We have focused at the effects of ending structures. The apex-vacuum barriers of the SWCNTs ended by -BH, -NH, and -O respectively have been obtained. The local field enhancement factor is affected by the atomic decoration significantly and is much smaller than the prediction of classical model for all three structures studied.

According to our simulations, the SWCNTs terminated by -BH and -NH clusters have lower turn-on fields than those terminated by oxygen atoms. In the same applied fields, the current of oxygen terminated SWCNT is weaker than the currents of SWCNTs terminated by -BH and

-NH clusters by an order or more. The simulation results suggest that the di-atom decorated SWCNT is more stable than H saturated SWCNT and has lower turn-on field than the oxygen saturated SWCNT. The orientation of the emission path depends on the applied field significantly.

**Acknowledgement.** The authors thank Chris J. Edcombe and Richard G. Forbes for the valuable discussions; and gratefully acknowledge the support from the National Natural Science Foundation of China (the Distinguished Creative Group Project; Grant No. 90103028, 90306016) and from Hong Kong Research Grant Council (HKU 7010/03P, HKU 7012/04P).

---

[1] W. B. Choi *et al.*, *Appl. Phys. Lett.* **75**, 3129 (1999).

[2] Collins, P. G.; Bradley, K.; Ishigami, M; Zettl, A. *Science* **287**, 1801-1804 (2000)

[3] (a) Kong, J.; Franklin, N. R.; Zhou, C.; Chapline, M. G.; Peng, S.; Cho, K.; Dai, H. *Science* **287**, 622-625 (2000) (b) Peng, S.; Cho, K. *Nanotechnology* **11**, 57-60 (2000)

[4] Chang, H.; Lee, J. D.; Lee, S. M.; Lee, Y. H. *Appl. Phys. Lett.* **79**, 3863-3865 (2001)

[5] N. de Jonge, Y. Lamy, K. Schoots, and T. H. Oosterkmp, *Nature* (London) **420**, 393 (2002).

[6] P.V. Semet *et al.*, *Appl. Phys. Lett.* **81**, 343 (2002).

[7] Mayer, A.; Miskovsky, N.M.; Cutler, P.H.; Lambin, Ph. *Phys. Rev. B* **68**,235401 (2003)

[8] Zheng, X.; Chen, G. H.; Li, Z.; Deng, S.; Xu, N. *Phys. Rev. Lett.* **92**, 106803 (2004)

[9] J. Peng, Z. Li, C. He, G. Chen, W. Wang, S. Deng, N. Xu, X. Zheng, G. Chen, C. Edgcombe, R. Forbes, preprint

[10] Lee, S. M.; An, K. H.; Lee, Y. H.; Seifert, G.; Frauenheim, T. J. *Am. Chem. Soc.* **123**, 5059-5063 (2001)

[11] Wadhawan, A.; Stallcup II, R. E.; Stephens II, K. F.; Perez, J. M. *Appl. Phys. Lett.* **79**, 1867 (2001)

[12] Amitesh Maiti, Jan Andzelm, Noppawan Tanpipat, and Paul von Allmen *Phys. Rev. Lett.* **87**, 155502 (2001)

[13] Zhi, C. Y.; Bai, X. D.; Wang, E. G. *Appl. Phys. Lett.* **81**,1690 (2002)

[14] Wadhawan, A. *et al.*, *Appl. Phys. Lett.* **79**,1867 (2001)

[15] Changwook Kim et al, *Phys. Rev. B* **68**,115403 (2003)

[16] Jhi, S.-H.; Louie, S. G.; Cohen, M. L. *Phys. Rev. Lett.* **85**, 1710 (2000)

[17] Zhu, X. Y.; Lee, S. M.; Lee, Y. H.; Frauenheim, Th. *Phys. Rev. Lett.* **85**, 2757 (2000)

[18] Park, N.; Han, S.; Ihm J. *Phys. Rev. B* **64**, 125401 (2001)

[19] Sorescu, D. C.; Jordan, K. D.; Avouris, Ph. *J. Phys. Chem. B* **105**, 11227 (2001)

[20] Moon, C.-Y.; Kim, Y.-S.; Lee, E.-C.; Jin, Y.-G.; Chang, K. J. *Phys. Rev. B* **65**, 155401 (2002)

[21] Steckel, J. A.; Jordan, K. D.; Avouris, Ph. *J. Phys. Chem. A* **106**, 2572 (2002)

[22] Grujicic, M.; Cao, G.; Gresten, B. *Appl. Surf. Science* **206**, 167 (2003)

[23] Gang Zhou, Wenhui Duan, Binglin Gu, *Phys. Rev. Lett.* **87**, 095504(2001)

[24] Changwook Kim, Yong Soo Choi, Seung Mi Lee, Joon T. Park, Bongsoo Kim, and Young Hee Lee, *J. Am. Chem. Soc.* **124**, 9906 (2002); Changwook Kim *et al.*, *Phys. Rev. B* **68**,115403 (2003)

[25] Mayer, A.; Miskovsky, N.M.; Cutler, P.H.; Lambin, Ph. *Phys. Rev. B* **68**,235401 (2003)

[26] Zheng, X.; Chen, G. H.; Li, Z.; Deng, S.; Xu, N. *Phys. Rev. Lett.* **92**, 106803 (2004)

[27] Jie Peng, Zhibing Li, Chunshan He, Xhaozhi Deng, Ningsheng Xu, Xiao Zheng, Guanhua Chen *Phys. Rev. B* **72**, 235106 (2005)

[28] Chu-Chun Fu, Jacques Dalla Torre, Francois Willaime, Jean-Louis Bocquet and Alain Barbu, *Nature* (London) **4**,68(2005)

[29] Rakwoo Chang, Gary S. Ayton, and Gregory A. Voth, *J. Chem. Phys.* **122**, 244716 (2005)

[30] Rao, A.M. *et al.*, *Science* **275**, 187 (1997); Blas, X. *et al.* *Phys. Rev. Lett.* **72**, 1878 (1994); Jishi, R. A.; Bragin, J.; Lou, L. *Phys. Rev. B* **59**, 9862 (1999).

[31] Wildo, J.W.G. Er *et al.* *Nature* (London) **391**, 59 (1998).

[32] Z.B. Li and W.L. Wang, *Chin. Phys. Lett.* **23**,1618 (2006).